J. Fluid Mech. (2011), *vol.* 681, *pp.* 340–369.
doi:10.1017/jfm.2011.203

Experiments and modelling of premixed laminar stagnation flame hydrodynamics

JEFFREY M. BERGTHORSON[1]†, SEAN D. SALUSBURY[1] AND PAUL E. DIMOTAKIS[2]

[1]Department of Mechanical Engineering, McGill University, Montreal, QC H3A 2K6, Canada

[2]Graduate Aeronautical Laboratories, California Institute of Technology, Pasadena, CA 91106, USA

(Received 17 June 2010; revised 20 April 2011; accepted 3 May 2011;
first published online 23 June 2011)

The hydrodynamics of a reacting impinging laminar jet, or stagnation flame, is studied experimentally and modelled using large activation energy asymptotic models and numerical simulations. The jet-wall geometry yields a stable, steady flame and allows for precise measurement and specification of all boundary conditions on the flow. Laser diagnostic techniques are used to measure velocity and CH radical profiles. The axial velocity profile through a premixed stagnation flame is found to be independent of the nozzle-to-wall separation distance at a fixed nozzle pressure drop, in accord with results for non-reacting impinging laminar jet flows, and thus the strain rate in these flames is only a function of the pressure drop across the nozzle. The relative agreement between the numerical simulations and experiment using a particular combustion chemistry model is found to be insensitive to both the strain rate imposed on the flame and the relative amounts of oxygen and nitrogen in the premixed gas, when the velocity boundary conditions on the simulations are applied in a manner consistent with the formulation of the streamfunction hydrodynamic model. The analytical model predicts unburned, or reference, flame speeds that are slightly lower than the detailed numerical simulations in all cases and the observed dependence of this reference flame speed on strain rate is stronger than that predicted by the model. Experiment and simulation are in excellent agreement for near-stoichiometric methane–air flames, but deviations are observed for ethylene flames with several of the combustion models used. The discrepancies between simulation and experimental profiles are quantified in terms of differences between measured and predicted reference flame speeds, or position of the CH-profile maxima, which are shown to be directly correlated. The direct comparison of the measured and simulated reference flame speeds, ΔS_u, can be used to infer the difference between the predicted flame speed of the combustion model employed and the true laminar flame speed of the mixture, ΔS_f^0, i.e. $\Delta S_u = \Delta S_f^0$, consistent with recently proposed nonlinear extrapolation techniques.

Key words: combustion, flames, laminar reacting flows

1. Introduction

The premixed flame stabilized in a stagnation point flow is a canonical combustion geometry that has been extensively studied in experiments and through analytical and numerical modelling approaches. Such laminar stagnation flames are stable and flat, allowing them to be modelled using a one-dimensional (1-D) axisymmetric

† Email address for correspondence: jeffrey.bergthorson@mcgill.ca

streamfunction approach that is an extension of planar Hiemenz flow (see Schlichting 1960; Sivashinsky 1976; Seshadri & Williams 1978). Due to advances in combustion research over the last 30 years, the basic laminar flamelet structure is now considered to be well-understood (Williams 2000; Law & Sung 2000). This progress was due to advances in large activation energy asymptotic methods (e.g. Durbin 1982), and the ability to numerically simulate flamelets with detailed chemistry and transport (e.g. Kee *et al.* 1988).

Sivashinsky (1976) solved for the location of a flame in an axisymmetric potential flow against a flat plate, and the constant axial velocity gradient that exists upstream of the flame is equal to the strain rate, or flame stretch imposed on the flame, due to the diverging streamlines in the flowfield (e.g. Law & Sung 2000). Experiments in jet-wall stagnation flows show that such flames can be modelled as a dual axisymmetric stagnation-point flow, where the first stagnation flow is towards an apparent plane determined by the flame dilatation, and the second flow impinges on the stagnation surface (Mendes-Lopes & Daneshyar 1985). The experimental data of Mendes–Lopes and Daneshyar were compared to theoretical predictions using large activation energy asymptotic methods by Eteng, Ludford & Matalon (1986) and Kim & Matalon (1988), through fitting of the potential flow model to the strain rate just upstream of the flame and inferring the flame speed as a fit parameter. Matalon, Cui & Bechtold (2003) extended the hydrodynamic theory of premixed flames and included solutions that account for variable transport properties through the flame and allow for variable Lewis number, but this formulation has not yet been compared to experimental data.

Including full transport and chemistry models with the 1-D hydrodynamic model allows the detailed simulation of strained premixed flames (Kee *et al.* 1988). While stagnation-point flames are widely used for estimating laminar flame speeds (e.g. Wang *et al.* 2009; Chong & Hochgreb 2011), or extinction strain rates (e.g. Egolfopoulos *et al.* 1997; Ji *et al.* 2010), relatively few comparisons of stagnation-flame simulations and experimental profiles are available. Law and co-workers studied methane–air flames using LDV and spontaneous Raman spectroscopy for velocity, temperature and major-species measurements, and reported general agreement for temperature and major species profiles when the flame location is adjusted to match the measurements (Law *et al.* 1994; Sung, Liu & Law 1996*b*). Bergthorson and Dimotakis showed that the 1-D model yields good agreement with experimental flame profile data if the boundary conditions are specified in a consistent manner, if the particle velocimetry method is modelled and if the combustion model employed predicts the flame speed accurately (Bergthorson & Dimotakis 2006, 2007).

This paper discusses several aspects of stagnation flame hydrodynamics that have not received previous study. Velocity profiles are measured for variable nozzle-to-plate separation distances to determine if the stagnation flame flowfield is insensitive to this distance, as found for non-reacting impinging laminar jets by Bergthorson *et al.* (2005*b*). The large activation energy asymptotic model for stagnation flames by Matalon *et al.* (2003) is extended to capture the experimentally observed velocity profile upstream of the flame. The analytical model and numerical simulations are compared to experiments where the flame strength is reduced using nitrogen dilution, and the pressure drop through the contraction nozzle is shown to be a controlling parameter on the resulting flowfield. The effect of varying the imposed strain rate on experimental flames is studied for methane and ethylene flames. Comparisons of measured and predicted velocity and CH radical profiles are used to assess analytical model and numerical simulation predictions, and differences in measured

and predicted flame position and reference flame speed are shown to be equivalent in the stagnation flame geometry.

2. Experiments

Experimental studies of stagnation flames have utilized a jet-wall configuration (e.g. Ishizuka *et al.* 1982; Egolfopoulos *et al.* 1997; Chong & Hochgreb 2011), or an opposed-jet stagnation flow (e.g. Ishizuka & Law 1982; Wang *et al.* 2009; Ji *et al.* 2010; Veloo *et al.* 2010). The jet-wall configuration results in non-adiabatic flames due to heat loss to the solid wall, while the opposed-jet configuration allows the study of essentially adiabatic flames due to the symmetry of the dual-flame configuration. Low-temperature stagnation walls introduce a heat sink to the flow, and for sufficiently large degrees of cooling, and sufficiently large rates of strain, extinction will occur (Durbin 1982; Libby & Williams 1983). Heat loss can also make the planar flame more robust to cellular instabilities, and impinging-jet flames are found to be more stable than those in the opposed-jet configuration (Egolfopoulos *et al.* 1997). Egolfopoulos *et al.* (1997) found that radical recombination at the wall is unimportant for wall temperatures below approximately 1000 K and that, even though flame extinction is largely controlled by the heat loss to the plate, the extinction strain rate is only weakly dependent on the wall temperature. The velocity minimum upstream of the flame is commonly referred to as the unburned or reference flame speed, S_u (e.g. Tien & Matalon 1991; Hirasawa *et al.* 2002). Egolfopoulos *et al.* (1997) showed that this reference flame speed, S_u, is independent of the wall temperature for flames well-separated from the wall.

The jet-wall geometry is chosen for this study due to the stability of the flames and the precise knowledge of the stagnation-point location and its associated boundary conditions. A schematic of the experimental apparatus is given in figure 1. Two different experimental apparatus were used in this study, one with a central premixed fuel-oxidizer jet with a diameter of $D = 9.9$ mm and the second with $D = 20$ mm. The nozzle to plate separation distance, L, is varied in these studies to determine its effect on the hydrodynamics. Nitrogen or helium is used as the co-flow gas to improve flame stability and prevent the flame from attaching to the nozzle rim (Ishizuka *et al.* 1982).

The premixed gas composition of fuel, air and, in some cases, nitrogen diluent is controlled using sonic metering valves on each supply line and monitoring the gas flow rate concurrently using Omega FMA thermal mass flow meters. The flow meters are calibrated using a Bios DryCal ML-500 dry piston calibrator and the resulting uncertainty in each flow rate is 0.6 %. In experiments with the larger diameter nozzle, the same functionality is obtained by using Brooks thermal mass flow controllers (5851S and 5850S). The gas streams are mixed in a mixing vessel upstream of the nozzle plenum and are seeded with micrometer-sized alumina particles for the velocimetry measurements.

In impinging jet flows, the static pressure drop across the nozzle, or Bernoulli pressure, Δp, determines the overall flowfield (Bergthorson *et al.* 2005*b*). This static pressure drop is measured using an electronic-capacitance manometer (BOC Edwards W57401100) and a temperature-stabilized 1 Torr full-scale differential pressure transducer (BOC Edwards W57011419). The differential pressure drop is used to calculate the Bernoulli velocity

$$U_B = \sqrt{\frac{2\Delta p/\rho}{1-(D/D_p)^4}}, \tag{2.1}$$

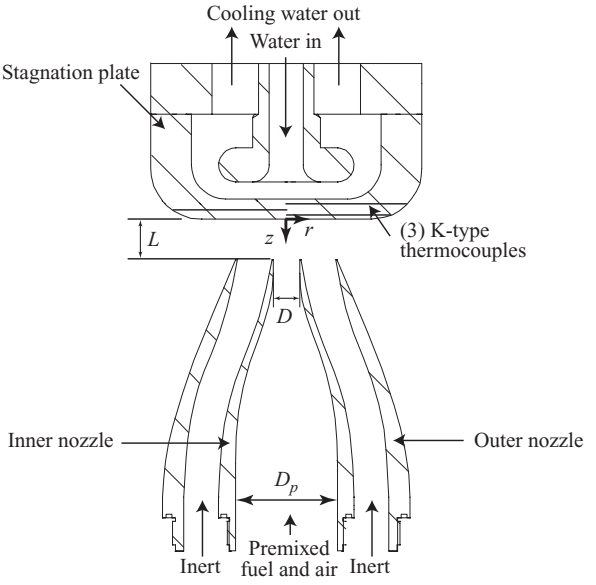

FIGURE 1. Schematic of stagnation flame experimental apparatus.

where ρ is the density of the jet fluid and $D_p = 38$ mm is the plenum diameter for the $D = 9.9$ mm nozzle (see figure 1).

The temperature of the stagnation plate is measured using K-type thermocouples located on the axis of the plate and the plate temperature is controlled by a valve on the water cooling line. Plate temperatures were held constant in each experiment near 350 K to prevent condensation on the plate surface. Mass flow, Bernoulli pressure and plate temperature data are recorded using National Instruments data acquisition hardware.

Two simultaneous laser diagnostic techniques are utilized to perform measurements in the stagnation flame experiments (Bergthorson, Goodwin & Dimotakis 2005*a*). Particle streak velocimetry (PSV) is utilized to measure axial velocity profiles along the nozzle centreline. Planar laser-induced fluorescence (PLIF) is used to measure relative concentration fields of the CH radical. Particle image velocimetry (PIV) is also used to measure two-dimensional (2-D) velocity fields in experiments with the larger nozzle diameter. Details on the laser diagnostic techniques are presented elsewhere and are omitted here for brevity (Bergthorson 2005; Bergthorson *et al.* 2005*a*; Bergthorson & Dimotakis 2007; Salusbury 2010).

3. Asymptotic model of stagnation flame hydrodynamics

Matalon and co-workers have developed a rigorous theory of premixed flames in stagnation flows (Eteng *et al.* 1986; Kim & Matalon 1988; Tien & Matalon 1991; Matalon *et al.* 2003). In these studies, the flame is treated as a gasdynamic discontinuity across which there is a jump in temperature, resulting in a drop in density and jump in the axial velocity (Matalon & Matkowsky 1982). Stagnation flames are subject to flame stretch due to the diverging streamlines of the stagnation flow field. This flame stretch is generally defined as $K = (1/A)\,[\mathrm{d}A/\mathrm{d}t]$ (Law 1988), which reduces, in a stagnation flow, to the strain rate, or velocity gradient, in the unburned gas upstream of the flame, $K = (\mathrm{d}u/\mathrm{d}z)_u$, where u is the axial velocity and z is the distance from the wall. In this paper, the hydrodynamic length scale, $L_h = S_f^0/K$,

is defined as the ratio of the laminar flame speed, S_f^0, and the experimentally imposed strain rate in the unburned gas upstream of the flame, K. The equations presented below have been re-normalized from those in the original articles using L_h as the fundamental length scale in the problem. These solutions are asymptotically valid as the ratio of the flame thickness, $L_D = \mathscr{D}_{th}/S_f^0$, to the hydrodynamic length scale becomes small, i.e. $\delta \equiv L_D/L_h \ll 1$, and the solution is presented as an expansion in powers of δ. In the flames studied here, the hydrodynamic length is of the order of 1 mm and the flame thickness is of the order 10^{-1} to 10^{-2} mm, leading to $0.05 < L_D/L_h < 0.1$.

The solutions are based upon a hydrodynamic model for stagnation flows that introduces a streamfunction to reduce the axisymmetric momentum equations to a single ordinary differential equation in the axial coordinate (see Appendix). The potential-flow boundary condition (Williams 2000) is used in the flame sheet modelling where the axial velocity profile becomes a linear function of distance from the virtual stagnation point and the unburned flowfield is irrotational. The velocity in the unburned region upstream of the flame in these models is thus given by:

$$\frac{u_u(z)}{S_f^0} = -\frac{(z-a)}{L_h}, \tag{3.1}$$

where a is the location of the virtual stagnation point, which is obtained directly from the unburned velocity profile and the flame location, d, as $a_0 = d_0 - L_h$ for the zeroth-order solution in δ. The solution of the differential equations solves the downstream velocity profile and the flame location, d, subject to the imposed jump conditions in velocity and temperature. The gasdynamic expansion across the flame sheet is given by $\sigma = \rho_u/\rho_b$, which is equal to $\sigma = T_b/T_u$ for a low-Mach number constant-pressure flame. In this expression, T_b is the burned temperature downstream of the flame and T_u is the unburned temperature upstream of the flame. The zeroth-order solution for d expanded in powers of δ is shown by Eteng *et al.* (1986) to be

$$\frac{d_0}{L_h} = \frac{2\sigma}{(\sigma^{1/2}+1)}, \tag{3.2}$$

and thus is a function only of the temperature ratio through the flame, σ, and the hydrodynamic length. Higher-order solutions for d are also presented in that paper, as well as in the work of Kim & Matalon (1988) and Matalon *et al.* (2003), the latter giving

$$\frac{d}{L_h} = \frac{d_0}{L_h} - \frac{L_D}{L_h}\left[\gamma_1 + \frac{\sigma^{1/2}-1}{\sigma^{1/2}+1}\,Pr\,\lambda_b + \frac{\sigma}{\sigma^{1/2}+1}\,le_{eff}\,\gamma_2\right], \tag{3.3}$$

for a flow with variable transport properties through the flame and variable Lewis number (for details, see Matalon *et al.* 2003).

The flame speed into the unburned mixture, S_f, at the location of the flame sheet is

$$S_f = S_f^0 - L_D\,K\,\alpha, \tag{3.4}$$

where α is the Markstein number, K is the flame stretch and S_f^0 is the laminar flame speed which depends only on the mixture composition, temperature and pressure for a chosen combustion chemistry model. The Markstein number depends only on the gas expansion parameter, σ, the Zel'dovich number, which is the activation energy scaled by the adiabatic flame temperature, and an effective Lewis number, which is a weighted average of the Lewis numbers of the excess and deficient reactants that depends on the reaction orders of the fuel and oxidizer and the equivalence ratio

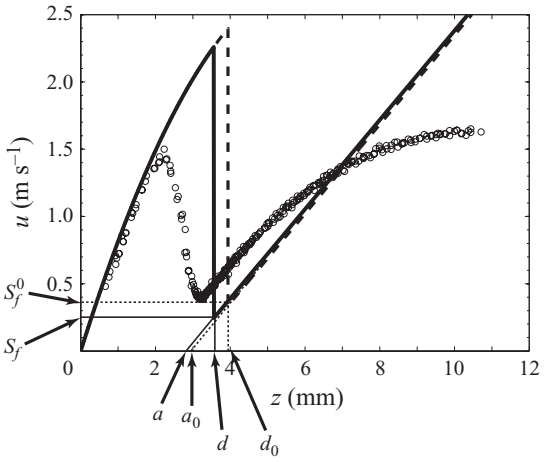

FIGURE 2. Comparison of zeroth-order model by Eteng *et al.* (1986) (dashed line) and higher-order model by Matalon *et al.* (2003) (solid line) to experimental data (○) for a $\Phi = 0.9$ CH_4–air flame with a strain rate of $K = 323\,\mathrm{s}^{-1}$ and $L = 12\,\mathrm{mm}$. The stagnation wall is at $z = 0$, the nozzle at $z = 12\,\mathrm{mm}$ and the flow is from right to left. The hydrodynamic length in these flows is $L_h = (d_0 - a_0) = S_f^0/K$.

(Matalon *et al.* 2003). The virtual stagnation point for the higher order solution is given by $a = d - L_h + L_D\,\alpha$.

With the flame and virtual stagnation point locations thus determined, the cold flow profile is fully specified with knowledge of the velocity gradient in the cold region, $(\mathrm{d}u/\mathrm{d}z)_u$. The velocity profile downstream of the flame in the burned region of the flow is given by

$$\frac{u_{b,0}(z)}{S_f^0} = -\left[\sigma^{1/2}\frac{z}{L_h} - \frac{1}{4}\frac{\sigma - 1}{\sigma}\left(\frac{z}{L_h}\right)^2\right] \tag{3.5}$$

to leading order (Eteng *et al.* 1986), and by

$$\frac{u_b(z)}{S_f^0} = \frac{u_{b,0}(z)}{S_f^0} + \frac{1}{8}\frac{L_D}{L_h}\frac{\sigma - 1}{\sigma^2}\left(Pr\lambda_b - \frac{1}{2}\sigma\, le_{eff}\,\gamma_2\right)\left(\frac{z}{L_h}\right)^2 \tag{3.6}$$

using higher order theory (Matalon *et al.* 2003). The hydrodynamic model captures the vorticity produced due to the baroclinic generation mechanism across the flame sheet that results in rotational flow downstream of the flame even though the upstream flow is irrotational.

Figure 2 compares the zeroth-order solution to the hydrodynamic flame model from Eteng *et al.* (1986) and the higher-order model by Matalon *et al.* (2003) to an experimental methane flame velocity profile at an equivalence ratio of $\Phi = 0.9$ and a separation distance of $L = 12\,\mathrm{mm}$. Flow is towards the plate in this geometry, resulting in negative velocities for the choice of the coordinate system used here ($z = 0$ at the wall). For convenience, $-u$ is plotted in all the figures in this paper to make the profiles positive. The only inputs to these models are the laminar flame speed, the temperature-dependent thermal conductivity, which is assumed to vary as $T^{1/2}$, the transport properties for the fuel and oxidizer that determine the Prandtl number and effective Lewis numbers, the temperature ratio across the flame, σ, the activation energy of the mixture, the reaction orders for the fuel and oxidizer and the velocity gradient upstream of the flame. The laminar flame speed for this slightly lean methane–air flame is $S_f^0 = 33.7\,\mathrm{cm\,s}^{-1}$, calculated with the CANTERA software package (Goodwin

2003) using the idealized model for an adiabatic, zero-stretch, 1-D flame (Grcar *et al.* 1986) and the GRI-Mech 3.0 combustion model (Smith *et al.* 1999). The transport properties are determined using CANTERA and the GRI-Mech 3.0 chemical kinetic and transport model and the temperature ratio across the flame is taken to be $\sigma = T_{ad}/T_u$, where the burned temperature is the adiabatic flame temperature, $T_{ad} = 2134\,\mathrm{K}$, calculated by an equilibrium thermodynamic calculation based on the unburned composition, pressure and temperature. The activation energy is $48.4\,\mathrm{kcal\ mol^{-1}}$ and the reaction orders are $a = -0.3$ for methane and $b = 1.3$ for oxygen in methane–air flames (Westbrook & Dryer 1981). Therefore, the only adjustable parameter in this model is the unburned velocity gradient, $K = 323\,\mathrm{s^{-1}}$, which is taken from a fit to the experimental data upstream of the flame in this preliminary implementation.

The zeroth-order solution has a flame velocity towards the unburned gas equal to the laminar flame speed of this methane–air mixture. The higher order solution of Matalon *et al.* (2003) reduces the flame speed due to the imposed flame stretch and the flame standoff distance is also reduced (see figure 2). Including variable transport properties leads to a first-order correction term in the standoff distance that is approximately 2.5 times larger than in the earlier model of Eteng *et al.* (1986). However, the predicted flame standoff distance is still larger than that experimentally measured (see figure 2). The reduction in the d value from the zeroth-order solution is primarily governed by the difference between the S_f and S_f^0 values normalized by the strain rate, K, leading to the cold flow profiles nearly collapsing with the difference in the location of the virtual stagnation point of the zeroth-order and first-order solutions being 0.1 mm (see figure 2). The velocity gradient in the post-flame region is accurately predicted by the model and is found to be controlled by the dominant term in the zeroth-order solution as $\sigma^{1/2}(\mathrm{d}u/\mathrm{d}z)_u$. The use of the potential flow solution for the cold velocity profile captures the observed shape of the experimental profile only for a short distance (2–3 mm) upstream of the flame and cannot capture the transition from a free jet (no gradient) to a stagnation flow (constant gradient) at a distance between 5 and 10 mm in figure 2, which corresponds to approximately 0.3 and $0.8D$ from the experimentally observed virtual stagnation point, a.

4. Extended analytical model of stagnation flame hydrodynamics

Velocity profiles in cold impinging jets are found to collapse for different values of the nozzle-to-plate separation distance, L, when normalized by the Bernoulli velocity, U_B (Bergthorson *et al.* 2005*b*). In order to assess the effect of this separation distance on premixed stagnation flames, experiments were performed for slightly lean ($\Phi = 0.9$) methane–air flames at constant U_B for different L values and the results are presented in figure 3. At constant U_B, the measured velocity profiles collapse independent of L/D as found for non-reacting impinging jets. Also included in figure 3 is the error function velocity profile that represents the non-reacting impinging-jet flow at the equivalent jet Reynolds number (Bergthorson *et al.* 2005*b*). The ignition of the flame results in the introduction of a virtual stagnation point that shifts the cold portion of the flow profile; however, the strain rate, $K = (\mathrm{d}u/\mathrm{d}z)_u$, upstream of the flame is unchanged. For smaller values of L, a velocity deficit and gradient are established at the nozzle exit such that the profiles match those for larger separations.

In non-reacting flows for values of $L/D \lesssim 0.4$, the stagnation pressure field will extend from the wall into the nozzle interior and begin to influence the acceleration of the flow within the nozzle contraction, leading to deviations from the self-similar profile (Bergthorson *et al.* 2005*b*). In a reacting stagnation flame, it is the distance from the nozzle to the virtual stagnation point that will determine whether the flow

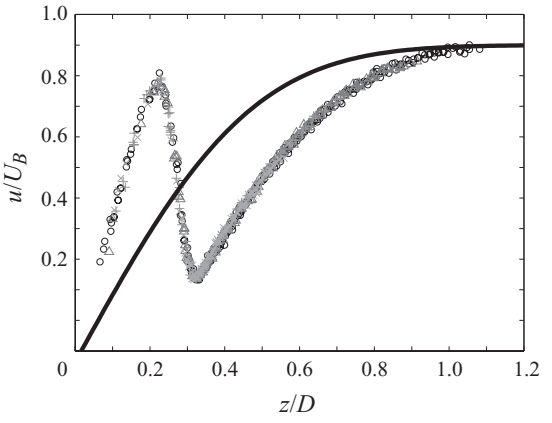

FIGURE 3. Methane–air flame profiles ($\Phi = 0.9$) for variable separation distances: $L/d = 0.6$ ($\times$), 0.8 (+), 1.0 ($\triangle$) and 1.2 ($\bigcirc$). Error function profile corresponding to cold impinging jet at same U_B (solid line) is included for comparison.

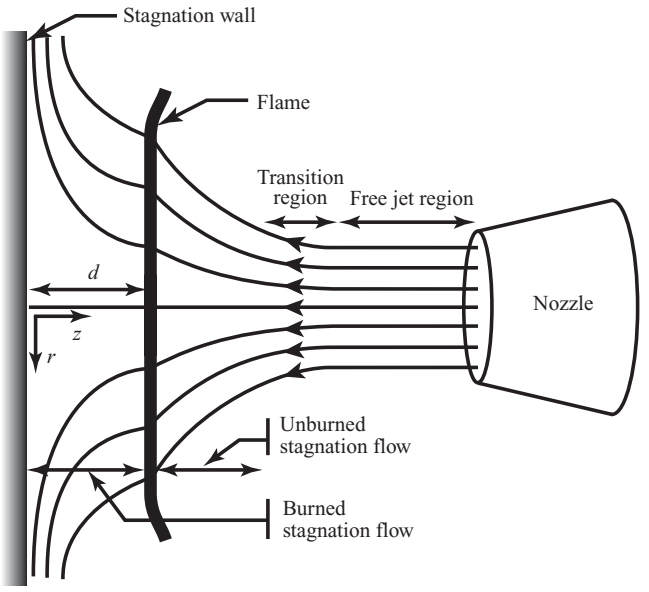

FIGURE 4. Schematic of the hydrodynamic model for stagnation flames generated from contraction nozzles (adapted from Matalon *et al.* 2003).

is self-similar. Thus, the nozzle-to-plate separation distance, L, is not an important parameter in these flames for $(L-a)/D \gtrsim 0.4$, as confirmed by the results in figure 3 where the profiles are seen to be self-similar for the experiment at $L/D = 0.6$, where $(L-a)/D \approx 0.39$. For $(L-a)/D \gtrsim 0.4$, the flame strain rate and resulting flame speed and location depend only on the imposed nozzle pressure drop and resulting U_B.

The stagnation flame hydrodynamic model by Matalon and co-workers can be extended based upon these new experimental results for jet-wall stagnation flames and analysis of the flowfield of non-reacting impinging laminar jets (Bergthorson *et al.* 2005*b*) to describe the entire flowfield of stagnation flames generated using contraction nozzles, as depicted in figure 4. This model is based upon that of Matalon *et al.* (2003) with the addition of the free jet and transition regions to the jet flow upstream of the

flame. The cold flow in the unburned region is well-described by the error function model developed for cold impinging jet flows (Bergthorson *et al.* 2005*b*)

$$u_{u,erf}(z) = U_B \,\mathrm{erf}\left[\frac{\alpha_{erf}}{D}(z - a_{erf})\right], \tag{4.1}$$

where α_{erf} is a non-dimensional parameter that determines the gradient and width of the error function profile and D is the nozzle diameter in the experiments. Bergthorson *et al.* (2005*b*) found that the α_{erf} parameter is a function of Reynolds number, $Re = \rho U_B D/\mu$, given by $\alpha_{erf}(Re) = 1.775 + 153/Re$ over the range $400 < Re < 1400$ with the numerical constants determined by least-squares fitting of the data. The virtual stagnation point for the error function, a_{erf}, is found by equating the cold-flow velocity profile to the flame speed, S_f, at the flame standoff distance, d, found from the higher order hydrodynamic model discussed above. Therefore, the cold-flow velocity profile is fully determined by the Bernoulli velocity, U_B, imposed upon the flame due to the dependence of α_{erf} on U_B.

The cold-flow error-function velocity profile allows the strain rate in the unburned region upstream of the flame to be determined from knowledge of the Bernoulli velocity. The velocity gradient of the error function model for the cold flow is described by a Gaussian, and thus there is not a unique strain rate to extract from the profile. In this work, the strain rate is determined by averaging the velocity gradient over a region from the flame location, d, to a point 30 diffusion lengths, L_D, upstream of the flame for methane–air flames and $40\,L_D$ for the ethylene–air flames discussed in this paper, which correspond to approximately 2 mm in both cases due to the smaller L_D value for ethylene flames. The chosen empirical constants lead to values of the strain rate that approximately match the values found from linear fits to the experimental velocity profiles and thus there is good agreement between the models and experiment. This method eliminates the need to fit experimental flame profiles to determine the flame location and velocity profiles from the analytical model, and thus the only communication between the analytical model and experiment is the measured Bernoulli velocity.

At the flame sheet location, d, the flow velocity rapidly increases as the density drops and the streamline curvature increases. The hot flow undergoes a secondary stagnation flow against the cold wall that is given by (3.6). However, this secondary stagnation flow is displaced away from the stagnation surface due to the presence of the viscous boundary layer at the wall. The viscous wall boundary-layer displacement thickness is given by (see Bergthorson *et al.* 2005*b*, Appendix B)

$$\delta_w = 0.80\sqrt{\frac{\nu}{(\mathrm{d}u/\mathrm{d}z)_b}}, \tag{4.2}$$

where the constant of 0.80 is determined by fitting the non-dimensionalized solution to the axisymmetric Hiemenz flow equations, ν is the kinematic viscosity of the gas and $(\mathrm{d}u/\mathrm{d}z)_b$ is the velocity gradient in the near-wall region. Due to the temperature gradient near the cold wall, held near 350 K in the experiments discussed here, the viscosity is set to its value in the unburned (cold) region of the gas. The velocity gradient can be determined from the solution of the hydrodynamic flame sheet equations to leading order as $(\mathrm{d}u/\mathrm{d}z)_b = \sigma^{1/2}(\mathrm{d}u/\mathrm{d}z)_u$. In the extended flame model presented in this paper, the wall boundary-layer displacement thickness is used to shift the entire flow profile upstream.

The flame sheet models treat the flame as a hydrodynamic discontinuity. In the actual flow, the finite flame thickness results in a smooth transition from the unburned to burned velocity profiles. Tien & Matalon (1991) show that this transition arises

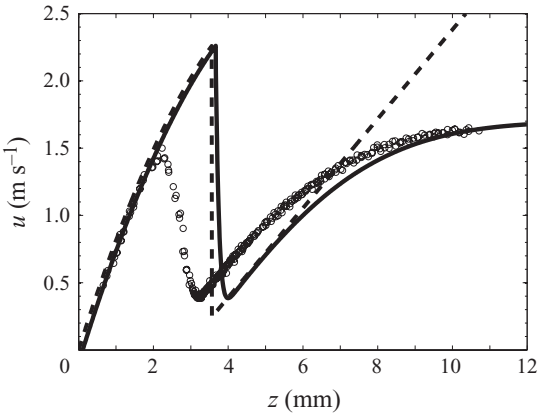

FIGURE 5. Comparison of analytical model by Matalon *et al.* (2003) (dashed line) with the extended model described in this paper (solid line) to experimental methane–air flame data (○) at $\Phi = 0.9$ and a measured Bernoulli velocity of $U_B = 1.7\,\mathrm{m\,s^{-1}}$.

primarily from the finite thickness of the temperature and density profiles. Their formulation is used to smooth the velocity profiles from the cold to hot region. In their method, they solve for the mass flux through the flame, $M = \rho u$. The axial velocity across the flame is given by $u(z) = M(z)/\rho(z) = [M(z)/\rho_u]\,[\rho_u/\rho(z)] = [M(z)/\rho_u]\,[\mathscr{T}(z)/T_u]$, where $\mathscr{T}(z)/T_u = T_b/T_u = \sigma$ for $z < d$ in the burned region, as above, and

$$\frac{\mathscr{T}(z)}{T_u} = \frac{\mathscr{T}_u(z)}{T_u} = 1 + q\exp^{-\zeta} + 2\delta[(1+q)\ln(1+q)\exp^{-\zeta} - (1+q\exp^{-\zeta}) \times \ln(1+q\exp^{-\zeta}) - (1-\alpha)q\zeta\exp^{-\zeta} - q\zeta^2\exp^{-\zeta}/2 - q\exp^{-\zeta}\mathscr{I}(\zeta)] \qquad (4.3)$$

for $z > d$ in the unburned region of the flow. In this expression, $\zeta = (z-d)/L_D$ is the distance from the flame sheet location scaled by the diffusion length, $q = \sigma - 1$ is the normalized amount of heat released within the flame and $\mathscr{I}(\zeta) = \int_{-\zeta}^{0} \ln\left(1 + q\exp^{\zeta}\right) \mathrm{d}\zeta$ (Tien & Matalon 1991). Therefore, in the present paper, the upstream flowfield of the extended analytical model has been adjusted to be

$$u_u(z) = \left\{ u_{u,erf}(z - \delta_w) + L_D K \ln\left[1 + q\exp\left(\frac{z - d - \delta_w}{L_D}\right)\right]\right\} \frac{\mathscr{T}_u(z)}{T_u}, \qquad (4.4)$$

which captures the preheat region of the flame where the velocity profile smoothly increases from the unburned to burned flow region.

A comparison of the model by Matalon *et al.* (2003) and the extension described in this paper that employs the cold flow error function velocity profile, the wall displacement thickness and the model of the preheat zone by Tien & Matalon (1991) are both presented in figure 5. The use of the cold flow error function eliminates the need to fit the velocity profile, replacing the strain rate as the model input parameter with the Bernoulli velocity, and is seen to capture the shape of the unburned region of the flow very accurately. Moreover, the use of the wall boundary-layer displacement thickness results in slightly improved agreement in the experimental and modelled velocity profiles in the burned region. The smoothing of the profiles in the flame region using the Tien & Matalon (1991) model captures the smooth flow profile in the unburned portion of the reaction zone that results in a velocity minimum upstream

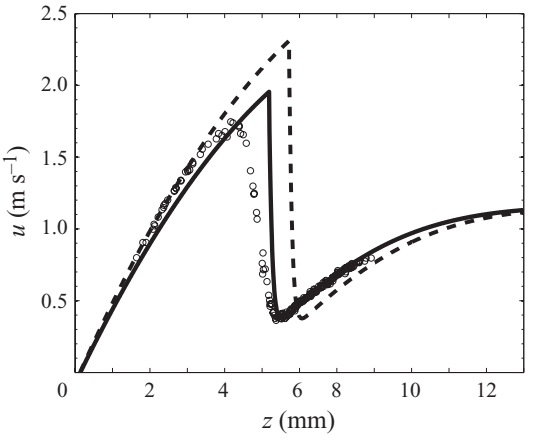

FIGURE 6. Comparison of extended analytical model using $\sigma = 7.11$ (dashed line) and $\sigma_{eff} = 6.03$ (solid line) to experimental methane–air flame data (○) at $\Phi = 0.9$ and $U_B = 1.16\,\mathrm{m\,s^{-1}}$.

of the flame. Figure 5 demonstrates that this velocity minimum upstream of the flame is determined by the flame speed, the imposed strain rate and the flame thickness.

As is observed in figures 2 and 5, the predicted flame standoff distance is higher than observed in experiment. The zeroth-order solution to the standoff distance depends only on the flame expansion parameter, σ, and the hydrodynamic length, $L_h = S_f^0/K$ (see (3.2)). In jet-wall stagnation flames, such as those discussed in this paper, the heat loss to the cold stagnation wall creates a thermal boundary layer that reduces the overall dilatation in the flowfield compared to that which would result under the adiabatic conditions assumed in the analytical model. In previous comparisons of experimental data to the analytical model, the measured maximum temperature was used to determine the burned temperature, T_b, required to calculate σ, leading to reasonable agreement in the predicted flame standoff distance (Eteng *et al.* 1986). Detailed simulation results are available for the flames studied in this paper, calculated using a streamfunction model for the hydrodynamics and detailed chemistry and transport properties (see next section). In order to calculate an effective gas expansion parameter for these flames, σ_{eff}, the first moment of the temperature profile is obtained from the detailed numerical simulations by integrating from the cold wall to the maximum temperature location and normalizing by T_u. The results of the model using the two different flame expansion parameters are compared to experiment for a stoichiometric methane flame at a large flame standoff distance in figure 6. Using a reduced value of the flame expansion parameter brings the predicted flame location into excellent agreement with experiment; however, the post-flame velocity gradient is slightly underpredicted. This is consistent with the previous results presented in Eteng *et al.* (1986), where the flame standoff location was accurately predicted but the post-flame velocity profile lies under the measured data. The reference flame speed values are changed by less than 0.3 % when σ_{eff} is used in place of σ, showing that the predicted S_u value is insensitive to the value of the gas expansion parameter. It is of interest to compare the predictions of the analytical model to experiment and detailed simulations with as few adjustable parameters as possible, and thus the adiabatic flame temperature will be used as T_b in the subsequent figures unless specified otherwise.

This new formulation of the analytical model, as well as detailed numerical simulations, will be compared to experimental results with varying nitrogen dilution

and imposed strain rates, or U_B, for methane- and ethylene–air flames in the following section.

5. Validation of analytical model and numerical simulations

The extended analytical model developed in this paper is validated against experimental data for methane and ethylene flames for different flame strengths and strain rates. The results of 1-D numerical simulations relying on a similar axisymmetric hydrodynamic streamfunction model for stagnation flames, but incorporating detailed chemistry, thermodynamic and transport models, are also validated against the experimental data. A detailed discussion of the numerical simulation approach is described in previous papers (Bergthorson *et al.* 2005*a*; Bergthorson & Dimotakis 2007) and in the Appendix. The simulations use a multi-component transport model (Kee, Coltrin & Glarborg 2003), and the GRI-Mech 3.0 (Smith *et al.* 1999), San Diego mechanism (2005, hereafter referred to as SD2005) and Davis, Law & Wang (1999, hereafter referred to as DLW99) chemical-kinetic models. The CANTERA simulations require that the inlet composition, inlet temperature and stagnation-wall temperature be specified (Kee *et al.* 2003). All necessary boundary conditions in the simulations are specified from experimental measurements, except that a no-flux (multi-component) boundary condition for species is assumed at the wall. A chemically-inert boundary condition is found to be appropriate for the cold wall temperatures used in this study (Egolfopoulos *et al.* 1997). The heat flux to the stagnation wall is accurately modelled in this approach, as the measured wall temperature is specified as a boundary condition in the numerical simulations. These simulations are able to accurately predict the measured velocity profiles, as well as the S_u and flame location, z_f, values, under conditions where the laminar flame speed predicted by the chemical-kinetic model is in agreement with experimental data (Bergthorson & Dimotakis 2007). The flame location, z_f, is specified as the location of the peak of the CH-radical profile, z_{CH}, obtained from numerical simulations and the experimental CH PLIF measurements.

The velocity and velocity gradient must be specified at the inlet of the simulation domain, $z = \ell$, in this formulation, where ℓ is a suitably chosen point upstream of the flame. The velocity, $u(\ell)$, and velocity gradient, $u'(\ell)$, are obtained from parabolic fits to the cold flow data upstream of the flame, minimizing errors in specifying these boundary conditions. A value of $\ell = 6\,\mathrm{mm}$ is used in the simulations in this section and simulation predictions are not sensitive to the choice of ℓ when a parabolic fit is used (see Appendix). In order to accurately compare the simulations with the velocimetry measurements, the experimental technique is modelled. The motion of a representative seeding particle through the flame is solved using a Lagrangian technique, accounting for particle inertia and thermophoresis (Sung, Law & Axelbaum 1994; Sung *et al.* 1996*a*), and yields the particle velocity profile. The resulting position–time record is then post-processed using the same methodology as in the PSV technique to estimate the modelled-particle-tracking (modelled-PT) profile (Bergthorson & Dimotakis 2006). The modelled-PT profile therefore accounts for particle inertia, thermophoretic and finite particle track interval effects. The approach used here is to simulate the experiment and its corresponding systematic uncertainties in order to allow direct comparison of model predictions with the experimental data, instead of attempting to correct the experimental profiles for the systematic effects. This manner of directly comparing numerical simulations to experimental data is an example of the 'paradigm shift' promoted by Connelly *et al.* (2009).

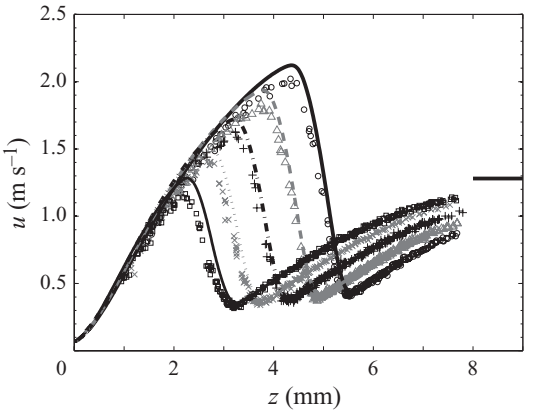

FIGURE 7. Comparison of stoichiometric methane–air flame data (symbols) to modelled-PT profiles from numerical simulations (lines) using GRI-Mech 3.0 for varying levels of nitrogen dilution ($\Phi = 1.0$). Oxygen content in the air of: 21.0 % (○ and solid line), 20.5 % (△ and dashed line), 20.0 % (+ and dash-dotted line), 19.5 % (× and dot line) and 19.0 % (□ and solid line). Horizontal line between $z = 8$ and 9 mm indicates U_B value.

5.1. *Variation of flame strength through dilution*

The addition of an inert diluent to a premixed flame will simultaneously reduce the gas expansion parameter, σ, and the laminar flame speed, S_f^0. This technique is used in this study in order to study the hydrodynamics of these flows for different flame strengths and to simultaneously validate the analytical model and numerical simulations. The level of dilution is presented as the molar percentage of the air (oxygen and nitrogen) that is made up of oxygen.

The detailed numerical simulations are compared to experimental data for stoichiometric methane flames with oxygen concentrations from 21 % (regular air) to 19 % in figure 7. Modelled-PT profiles are compared to experiments and the simulations are performed using the GRI-Mech 3.0 model. The simulated results show good agreement with experiment in each case, with the simulated profiles falling slightly above the experimental measurements. The Bernoulli velocity is constant in these experiments to within 1 %. With increasing dilution, the laminar flame speed and the temperature of the burned gas, and thus $\sigma = T_b/T_u$, are reduced which results in a decrease in the flame standoff distance from the stagnation wall. The strain rate, $(\mathrm{d}u/\mathrm{d}z)_u$, upstream of the flame varies by less than 2.5 % for constant Bernoulli velocity. This is evident from the parallel nature of the curves upstream of the flame and the collapse of the profiles in the near-wall region. The velocity profiles collapse in the burned region because this profile is determined by the strain rate upstream of the flame, which is constant for constant Bernoulli velocity, and the gas expansion parameter (see (3.5)). Figure 7 also highlights the importance of specifying the velocity boundary conditions for simulations from fits to the velocity data. For these five flames, the velocity profiles and actual nozzle-exit velocities are very different from each other due to the different flame stand-off distances, even though the U_B values are held constant.

A comparison of the velocity profiles predicted using the analytical model with σ_{eff} to experiment is given in figure 8. The reference flame speeds are adjusted by approximately 0.3 % when σ_{eff} is used in place of σ. The Markstein number, α, varies for these diluted flames from 4.5 at 21 % O_2 to 4.4 at 19 % O_2. The accurate prediction of flame location and reference flame speed for the non-diluted flame is visible, but

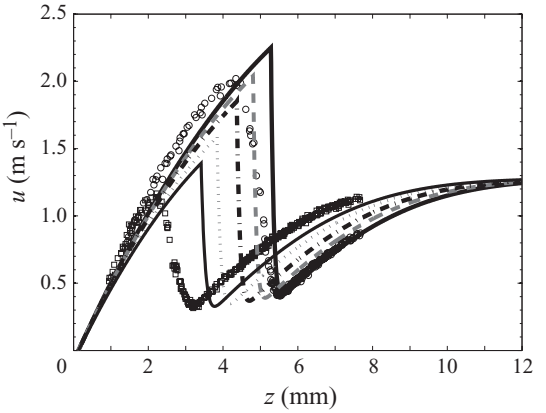

FIGURE 8. Comparison of stoichiometric methane–air flame profiles (symbols) to analytical model (lines) using σ_{eff} for varying levels of nitrogen dilution ($\Phi = 1.0$). Oxygen content in the air of: 21.0 % (○ and solid line), 20.5 % (dashed line), 20.0 % (dash-dotted line), 19.5 % (dotted line) and 19.0 % (□ and solid line). Only the non-diluted and highest-dilution experimental profiles are included for clarity.

larger error in the predicted flame location can be seen for smaller d values which are associated with higher dilution levels. This is expected as the non-dimensional parameter, L_D/L_h, increases as d decreases, making the assumption that $L_D/L_h \ll 1$ less valid. Use of σ_{eff} in the analytical model, however, prevents the collapse of the post-flame velocity profiles, and the associated velocity gradient, that is observed both in experiment and in detailed simulations in figure 7. The extended analytical model predicts that, for constant U_B, the velocity profiles will be a family of curves with decreasing virtual stagnation points as the dilution level is increased, as is observed (compare figures 7 and 8). The fact that the strain rate depends only on the imposed Bernoulli velocity, and not the flame speed, flame position or the nozzle to plate separation distance (see figures 3, 7 and 8) has important implications for extinction strain rate studies where uncertainty in the upstream velocity boundary conditions in numerical simulations leads to large uncertainties in the predicted extinction strain rates (e.g. Ji *et al.* 2010).

5.2. *Variation of strain rate for methane and ethylene flames*

Another important parameter in stagnation flame studies is the strain rate, K, imposed upon the flame. This parameter is varied in the experiments by directing a larger portion of the premixed gas stream to the nozzle, resulting in a higher jet velocity, and U_B, that pushes the flame towards the stagnation wall. Lean, stoichiometric and rich flames of methane, ethane and ethylene have been studied over the range of strain rates for which flames can be stabilized in this geometry (see Bergthorson 2005). For low jet velocities, the flames will stabilize on the nozzle rim (Ishizuka *et al.* 1982) and will not be well-represented by the stagnation flow model relied on in this work. At large jet velocities, the strain rate will exceed the extinction strain rate and the flame will be extinguished.

To illustrate the effect of strain rate, experimental data and modelled-PT profiles obtained from the simulations are compared for slightly-lean methane flames in figure 9. The simulated profiles lie slightly above the data in the post-flame region in all cases, indicating that the flame speed predicted by GRI-Mech 3.0 is slightly higher than observed in the experiments. Small velocity differences upstream of the flame

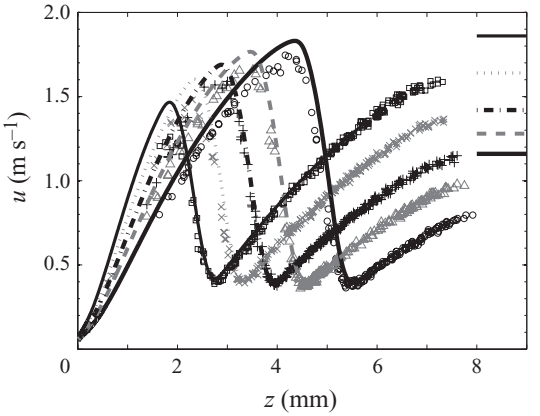

FIGURE 9. Lean ($\Phi = 0.9$) methane–air profiles for variable imposed strain rate. PSV data indicated with symbols, and modelled-PT profiles from numerical simulations using GRI-Mech 3.0 shown with curves for strain rates, $(\mathrm{d}u/\mathrm{d}z)_u$, of: 218 s^{-1} (○ and solid line), 236 s^{-1} (△ and dashed line), 270 s^{-1} (+ and dash-dotted line), 325 s^{-1} (× and dotted line) and 370 s^{-1} (□ and solid line). Horizontal lines between $z = 8$ and 9 mm indicate U_B values.

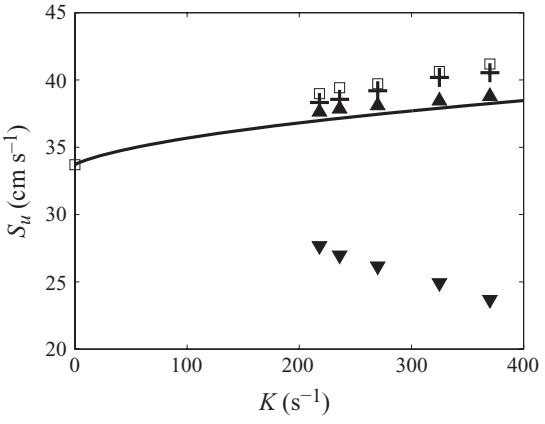

FIGURE 10. Reference flame speeds from measurements (+), numerical simulations (□), extended analytical model results (▲) and model by Tien & Matalon (1991) (solid line) for lean methane–air flames, $\Phi = 0.9$, at variable strain rates. Laminar flame speed (□) at $K = 0$ and the S_f values (▼) are also included for reference.

are magnified in the post-flame region because of the large drop in density across the flame that results from the combustion heat release, allowing sensitive assessment of the model performance (Bergthorson & Dimotakis 2006). The level of agreement between simulation and experiment for variable strain rate is consistent, indicating that the hydrodynamic model can capture this effect if the flame speed is accurately predicted by the chemistry model employed.

A summary of predicted and measured flame speeds and position data are presented in figures 10 and 11, respectively. The laminar flame speed for this $\Phi = 0.9$ methane–air flame is calculated using CANTERA and the GRI-Mech 3.0 chemistry model to be 33.7 cm s^{-1} and the adiabatic flame temperature is 2134 K. As the flow rate to the nozzle is increased, the Bernoulli velocity increases and the flame is pushed towards the stagnation wall (see figure 9). The numerical simulation values are slightly higher than experiment in all cases, consistent with the profile comparisons shown in figure 9. The

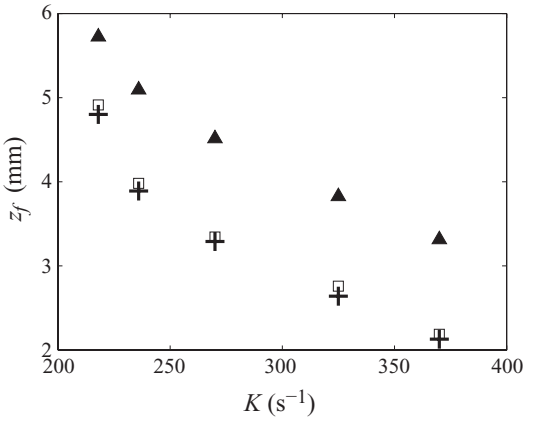

FIGURE 11. Flame positions from measurements (+), numerical simulations (□) and extended analytical model results (▲) for lean methane–air flames, $\Phi = 0.9$, at variable strain rates.

analytical model results are slightly below the experimental values, with the predicted variation in S_u with strain rate being slightly weaker than observed in the experiment and detailed numerical simulations. Also included in figure 10 is the prediction of S_u versus strain using the model by Tien & Matalon (1991), which shows a nonlinear variation of the reference flame speed with strain rate and falls below the experimental measurements. The slight difference between the solid model curve and the discrete analytical model points results from the use of a linear cold velocity profile in the Tien & Matalon (1991) curve and the error function model in the present paper.

A decrease in the flame speed, S_f, with increasing strain rate is observed in the model through the flame speed equation for the positive Markstein numbers associated with all flames in this study (see (3.4)). The Markstein number for these slightly lean methane flames is 4.1, and the linear decrease of S_f with increasing K is clearly visible in figure 10. In contrast, the observed velocity minima upstream of the flame, S_u, increase with increasing strain rate (see figures 9 and 10). For all of the flames studied in this paper and in Bergthorson (2005), increasing strain rate results in increased unburned reference flame speed, S_u. This is in accord with the discussion by Tien & Matalon (1991), who showed that while the flame speed decreases with increasing strain for stoichiometric methane–air flames, the velocity minimum increases due to the effect of the temperature and density profiles. The flame thickness is fairly constant for large changes in flame strain rate (Tien & Matalon 1991), and thus the temperature profile acts as a low-pass filter that smoothes the transition from the unburned to burned velocity profiles (see, for example, figure 5). The steepening gradients as strain rate is increased are averaged out and the result is an increase in S_u while the flame speed, S_f, decreases. The shallower slope of the S_u versus K curve predicted by the analytical model is likely due to an underprediction of the actual thickness of the preheat zone observed in the experimental and simulated flames.

Recently, Egolfopoulos and co-workers have developed a method for determining the laminar flame speed from stretched flame speed data that involves a nonlinear extrapolation technique (Wang *et al.* 2009; Ji *et al.* 2010; Veloo *et al.* 2010). Numerical simulations using a formulation similar to that in this study are used to simulate the effect of stretch on the reference flame speed, S_u, from strain rates of the order of $60\,\mathrm{s}^{-1}$, below which heat loss to the upstream boundary introduces additional

uncertainty, to values above the highest strain data available (Wang *et al.* 2009). The simulated values of S_u versus K are nearly linear over this strain rate range, but the intercept of a linear extrapolation would lie above the laminar flame speed that is predicted by the same combustion chemistry model used to simulate the strained S_u values (Wang *et al.* 2009), as seen in the current results in figure 10. Therefore, these authors fit a high-order polynomial to the simulated data that passes through the simulated S_u values and the laminar flame speed, S_f^0. This polynomial shows a nonlinear variation in the region from $K = 0$ to between $K = 60$ and $K = 150\,\mathrm{s}^{-1}$, depending on the strength of the flames studied (Wang *et al.* 2009; Ji *et al.* 2010; Veloo *et al.* 2010). In order to find the laminar flame speed value from the experimental data, the high-order polynomial is shifted vertically until the simulated S_u values at each strain rate fit the experimental data in a least-squares sense. The vertical shift of the polynomial is justified because the shape of the simulated S_u versus K curve is not strongly affected by changes in key reaction rates or fuel and oxygen diffusivity (Wang *et al.* 2009), the actual value of the predicted laminar flame speed (Ji *et al.* 2010) or the details of the chemistry model used (Veloo *et al.* 2010). These authors also suggest that the use of detailed simulations including full kinetics and transport will provide a more accurate prediction of the variation of S_u with strain rate. This is confirmed by the results of figure 10, where the numerical simulations are seen to predict the same variation of S_u with K as observed in experiment, which is steeper than that predicted by the analytical model. The use of a vertical shift of a nonlinear extrapolation function to determine the laminar flame speed relies on an assumption that differences between simulated and measured reference flame speeds, $\Delta S_u = \left(S_{u,sim} - S_{u,exp}\right)$, are equal to differences between the simulated and true laminar flame speeds, $\Delta S_f^0 = \left(S_{f,sim}^0 - S_{f,true}^0\right)$.

In figure 11, the analytical model is seen to capture the variation in the flame position as the Bernoulli velocity increases, but the values are consistently higher than experiment, as discussed previously. The only model parameter that is varied for the five model profiles is U_B. The simulated results are in close agreement with, but slightly larger than, the experimental measurements, consistent with the results for the S_u values in figure 10.

Lean ethylene–air experimental data for increasing U_B and strain rate are compared to numerical simulations using the DLW99 mechanism in figure 12. It can be observed that the flame speed predicted by the DLW99 model is lower than that observed experimentally for these lean ethylene flames, with the simulated flame profiles falling below those experimentally measured. The largest deviations are observed near the velocity maxima in the burned region due to the amplification of small differences in the upstream values due to the heat release, as discussed previously. The simulated velocity profiles are constrained by the fixed velocity and velocity gradient value at the simulation inlet, $z = \ell$, causing the differences between predicted and observed flame speeds to be manifested in different locations and values of the velocity minima upstream of the flame and deviations in the post-flame velocity profiles. The simulated flame for the highest strain case is significantly weaker than experimentally measured, indicating that the model is predicting near-extinction conditions earlier than observed in the data. However, the data for the highest strain-rate flame also shows that the S_u value is not increasing with strain as for the other four flames, indicating that the reference flame speed for this flame is being affected by heat loss to the wall, unlike the results for flames well-separated from the wall. The DLW99 model predicts a laminar flame speed of $S_f^0 = 35.2\,\mathrm{cm\,s}^{-1}$ for these lean ethylene flames at $\Phi = 0.7$. In contrast, the SD2005 model predicts a laminar flame speed of $S_f^0 = 40.7\,\mathrm{cm\,s}^{-1}$ at

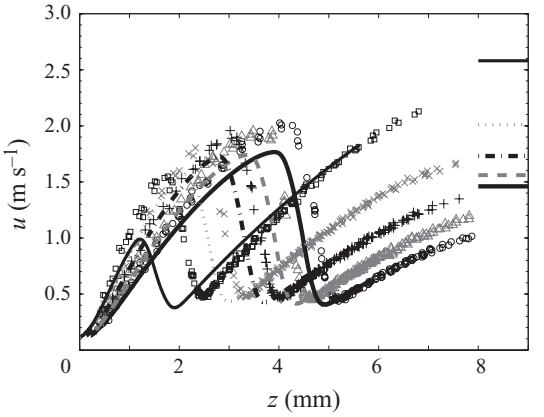

FIGURE 12. Lean ($\Phi = 0.7$) ethylene–air profiles for variable imposed strain rate. PSV data indicated with symbols, and modelled-PT profiles from numerical simulations using DLW99 mechanism shown with curves for strain rates, $(\mathrm{d}u/\mathrm{d}z)_u$, of: 251 s^{-1} (○ and solid line), 285 s^{-1} (△ and dashed line), 328 s^{-1} (+ and dash-dotted line), 370 s^{-1} (× and dotted line) and 492 s^{-1} (□ and solid line). Horizontal lines between $z = 8$ and 9 mm indicate U_B values.

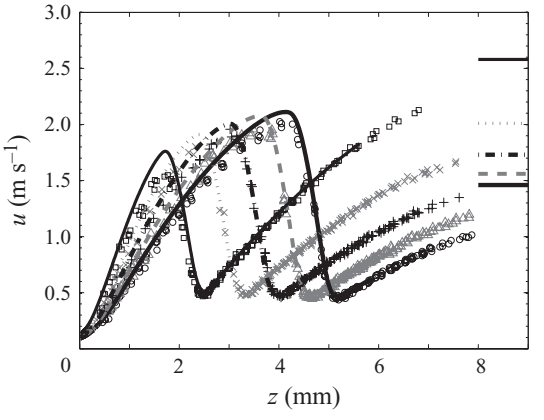

FIGURE 13. Lean ($\Phi = 0.7$) ethylene–air profiles for variable imposed strain rate. PSV data indicated with symbols, and modelled-PT profiles from numerical simulations using the SD2005 mechanism shown with curves. Legend as in figure 12.

$\Phi = 0.7$ for ethylene–air flames and modelled-PT velocity profiles using this model are in close agreement with experimental data, as shown in figure 13, with post-flame velocity profiles falling slightly above the data.

Figures 14 and 15, respectively, show a comparison of modelled and simulated flame speeds and positions to experimental data. In the model results for ethylene flames, the transport properties and adiabatic flame temperature, $T_{ad} = 1997$ K, are calculated using CANTERA and the GRI-Mech 3.0 mechanism. The activation energy is 30 kcal mol^{-1} and the reaction orders are $a = 0.1$ for ethylene and $b = 1.65$ for oxygen in ethylene–air flames (Westbrook & Dryer 1981). The resulting Markstein number for these lean ethylene flames is 4.49. In figure 14, it is observed that the higher laminar flame speed predicted by the San Diego mechanism leads to better agreement with experiment for flames at all strain rates for both the analytical model and numerical simulation results, with the simulated values falling above the analytical model values

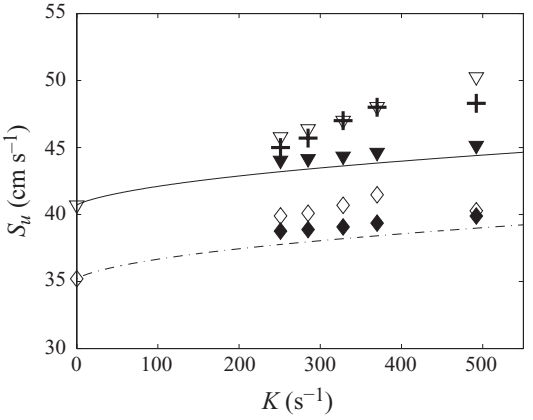

FIGURE 14. Reference flame speeds from measurements (+), numerical simulations using SD2005 (▽) and DLW99 (◇) chemistry models, extended analytical model results using SD2005 (▼) and DLW99 (◆) models and model by Tien & Matalon (1991) using SD2005 (solid line) and DLW99 (dash dotted line) models for lean ethylene–air flames, $\Phi = 0.7$, at variable strain rates. Simulated laminar flame speed values using the respective mechanisms are also included for reference.

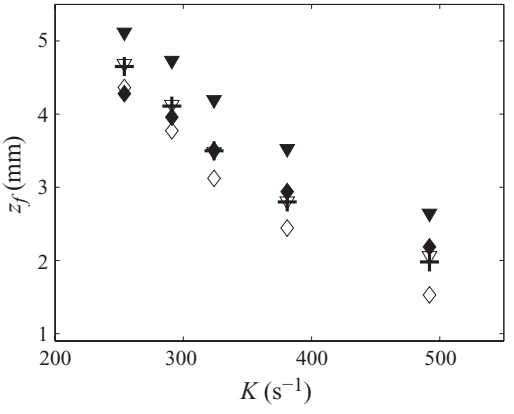

FIGURE 15. Flame positions from measurements (+), numerical simulations using SD2005 (▽) and DLW99 (◇) chemistry models and extended analytical model results using SD2005 (▼) and DLW99 (◆) models for lean ethylene–air flames, $\Phi = 0.7$, at variable strain rates.

as discussed for methane flames and shown in figure 10. The observed variation of S_u with strain rate is well-captured by the detailed numerical simulations, while the predicted trend is weaker in the analytical model results. The predicted flame speed for the highest strain case is significantly lower than measured, due to the fact that the DLW99 model is predicting a near-extinction flame, as discussed previously in the context of figure 12. The SD2005 model predicts flames that are in good agreement with experiment in both figures 13 and 14, except for the highest-strain case. The highest-strain experimental flame is being affected by wall heat-loss, and this effect is over-predicted by the DLW99 model and under-predicted by the SD2005 model, consistent with the fact that they under- and slightly over-predict, respectively, the flame speeds observed in experiment.

The predicted flame positions using SD2005 are upstream of measurements for the analytical model and in good agreement with the data for the simulations (see

figure 15) as found for methane flames (cf. figure 11). The numerically simulated values of the flame position are downstream of the measurements using the DLW99 model, while the analytical model values are close to the experimental data due to a fortuitous cancellation of errors.

A similar level of agreement between simulation and experiment for both methane and ethylene flames of various strain rates indicates that the 1-D hydrodynamic equations and combustion chemistry models used in the numerical simulations accurately account for this effect when the boundary conditions are specified from parabolic fits to the cold-flow portion of the data (see Appendix). The results presented here and additional results by Bergthorson (2005) show that the imposed strain rate is not a factor in determining the relative agreement between simulations and experiment for the range of strain rates achievable in the jet-wall geometry. This result is important, as it indicates that a comparison of a single experimental profile with numerical simulation is sufficient to assess the prediction of the flame speed by a specific combustion chemistry model. If the predicted laminar flame speed is in agreement with the true laminar flame speed of the mixture, the experimental and simulated profiles will collapse. Deviation of the prediction from the true laminar flame speed leads to disagreement throughout the profile, which can be quantified using the values of the velocity minima, S_u, velocity maxima or flame location, as discussed in the next section.

5.3. *Quantitative assessment of model and simulation performance*

Such experiments provide detailed velocity and species profile data that can be compared with model predictions. Comparisons of experimental and simulated velocity profiles for methane, ethane and ethylene flames under lean, stoichiometric and rich conditions are available elsewhere (Bergthorson & Dimotakis 2007) and provide a visual means of validating the predictions of different models. However, it is desirable that specific quantitative measures be extracted from such profiles to be used as validation or optimization targets for chemical kinetic models.

Variations between experimental data at multiple equivalence ratios using a selection of chemistry models were previously quantified by comparing the difference between measured and predicted CH-layer locations (Bergthorson *et al.* 2005*a*; Bergthorson & Dimotakis 2007). The difference between simulated (*sim*) and experimental (*exp*) CH peak locations, $\Delta z_{\mathrm{CH}} = z_{\mathrm{CH},sim} - z_{\mathrm{CH},exp}$, is normalized by the simulated CH-layer thickness, δ_{CH}, calculated using the SD2005 model at stoichiometric conditions. The CH-layer thickness has a value of $\delta_{\mathrm{CH}} \approx 2L_D$ for stoichiometric methane- and ethylene–air flames and is not sensitive to the choice of chemistry model used, indicating that the width of the CH-layer at $\Phi = 1$ is controlled by the diffusion of radicals upstream and downstream from the narrow location at which they are produced within the flame.

One quantity that has been extensively used in combustion model validation is the laminar flame speed, which cannot be measured directly and requires that multiple strained flame measurements be extrapolated to zero stretch (see Tien & Matalon (1991); Hirasawa *et al.* (2002); Wang *et al.* (2009); Ji *et al.* (2010); Veloo *et al.* (2010); Chong & Hochgreb (2011) and references therein). Uncertainties arise in these extrapolations depending on whether linear or nonlinear techniques are used, and these uncertainties can be as high as 20 % under rich conditions (Ji *et al.* 2010). In this work, the reference flame speed, S_u, can be modelled directly, thereby alleviating the need for such extrapolations. As discussed above, the numerical simulations accurately predict the variation of the S_u values with strain rate (Wang *et al.* 2009; Ji *et al.* 2010;

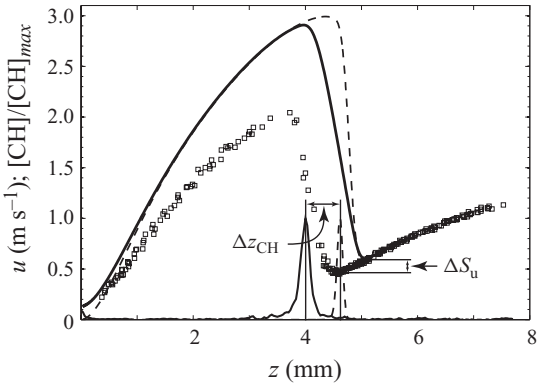

FIGURE 16. Measured and computed velocity and CH radical profiles for a diluted (17 % O_2) $\Phi = 1.0$ ethylene flame using GRI-Mech 3.0. PSV data (□), simulated fluid velocity (dashed line), modelled-PT profile (solid line), PLIF data (solid line) and simulated CH profile (dashed line) are included.

Veloo *et al.* 2010), and therefore differences in reference flame speeds from experiment and simulation are directly proportional to the differences between the true laminar flame speed of the mixture and that predicted by the combustion chemistry model used in the numerical simulations, $\Delta S_u = \Delta S_f^0$. The direct comparison of detailed model predictions that account for the systematic effects inherent in any experimental measurement technique can result in reduced experimental uncertainty when comparing numerical models to experiment, as demonstrated by Connelly *et al.* (2009).

Figure 16 shows a comparison between data and simulation for a diluted stoichiometric ethylene flame using GRI-Mech 3.0. GRI-Mech 3.0 was not developed to model ethylene kinetics and predicts a flame speed that is significantly higher than measured, resulting in a simulated flame that is upstream of the measurements. This example was specifically chosen because of the clear discrepancies exhibited between simulated and experimental profiles. The difference between simulation and experiment in these flames can be quantified by the difference in reference flame speeds, $\Delta S_u = S_{u,sim} - S_{u,exp}$, or the difference in CH-radical profile peak locations, $\Delta z_{\mathrm{CH}} = z_{\mathrm{CH},sim} - z_{\mathrm{CH},exp}$, as shown in figure 16. Differences in the maximum velocity downstream of the flame could also be used, but these contain higher uncertainty due to the need for thermophoretic and velocimetry-resolution corrections to simulated velocity profiles in this region (see figure 16 and Bergthorson & Dimotakis (2006)).

In the stagnation-flame geometry, differences in flame position and flame speed are directly correlated. The strain rate of the flow is the velocity gradient directly upstream of the flame, $(\mathrm{d}u/\mathrm{d}z)_u$. As the velocity profile just upstream of the flame is well approximated by a linear gradient, differences in flame, or z_{CH}, position and flame speed can be related through

$$\Delta S_u \approx (\mathrm{d}u/\mathrm{d}z)_u \, \Delta z_{\mathrm{CH}}. \tag{5.1}$$

The analytical model of Matalon and co-workers also shows a linear dependence of the flame position on the flame speed, as d is scaled by the hydrodynamic length, L_h, which is defined as the ratio of the flame speed to the velocity gradient upstream of the flame, i.e. $L_h = S_f^0/K$. Figure 17 shows the normalized differences between numerical simulation predictions and experimental measurements of the CH-profile peak locations, $\Delta z_{\mathrm{CH}}/\delta_{\mathrm{CH}}$, and reference flame speeds, $\Delta S_u / [(\mathrm{d}u/\mathrm{d}z)_u \, \delta_{\mathrm{CH}}]$,

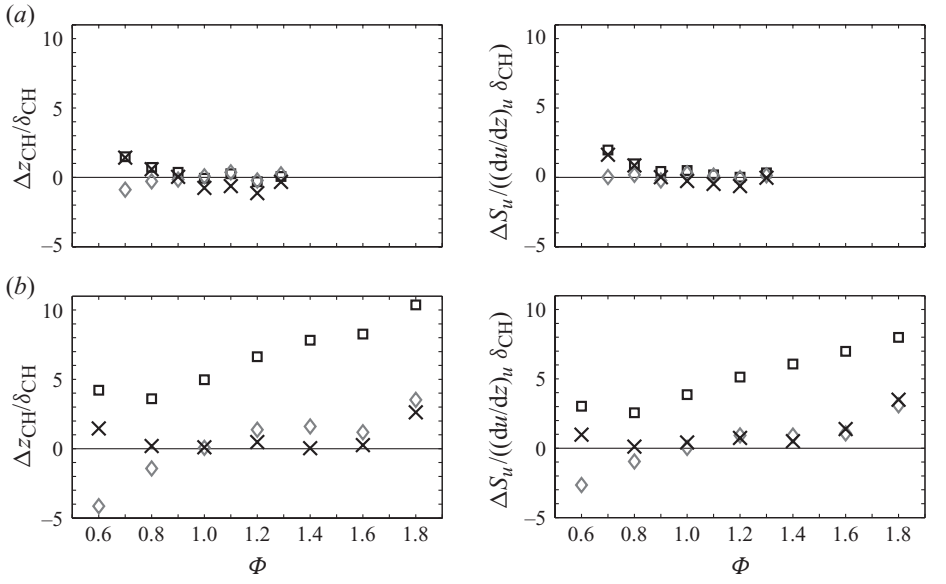

FIGURE 17. Difference between simulated and measured CH-peak locations (left) and reference flame speeds (right) for: (*a*) methane–air and (*b*) ethylene flames. Chemical kinetic models used: GRI-Mech 3.0 (□), DLW99 (◇) and SD2005 (×). The total experimental uncertainty in $\Delta z_{CH}/\delta_{CH}$ is approximately ± 0.5.

for methane and ethylene flames. The ethylene flames studied here were diluted near stoichiometric conditions to achieve similar flame locations with similar values of the Bernoulli velocity (see Bergthorson & Dimotakis (2007) for compositions). These dilution levels do not affect the performance of the model as compared to experiment, as shown in figure 7 for diluted methane flames. The ΔS_u values are normalized using (5.1) and δ_{CH} so that the two plots can be compared on the same scale. Positive values of $\Delta z_{CH}/\delta_{CH}$ or $\Delta S_u/\left[(\mathrm{d}u/\mathrm{d}z)_u\ \delta_{CH}\right]$ indicate that the simulated CH profile is upstream of the PLIF profile and that the predicted flame speed is higher than experiment. A comparison of the normalized Δz_{CH} and ΔS_u values in figure 17 shows that the two different metrics for simulation performance yield equivalent results. The results indicate that the flame speed predicted by the GRI-Mech 3.0 or SD2005 combustion models are in good agreement for methane flames, but slightly higher than observed for lean conditions. The DLW99 model shows good agreement for methane flames. For ethylene flames, the SD2005 model gives the closest agreement with experiment, while the DLW99 mechanism predicts significantly lower flame speeds and positions than measured for lean flames. GRI-Mech 3.0 was not developed to model ethylene flames and predicts significantly higher flame speeds than measured in all cases. These results are included to show the consistency of the two different metrics for model performance used in this paper for cases with significant deviations between experiment and simulation. As the ΔS_u values get large, the approximation that the flow is linear upstream of the flame will not hold and the two measures deviate slightly from each other. However, either experimental metric provides an accurate target for combustion model validation. The uncertainty in boundary-condition measurements is propagated through simulations and results in a total estimated uncertainty in predicted flame location of $\approx \pm 0.5\,\delta_{CH}$ (Bergthorson 2005). This uncertainty is much lower than the observed maximum variations between

the different models and experiment in figure 17. Experiments using the technique described in this paper to study propane–air and propylene–air flames also find a good correlation between differences in reference flame speeds or CH-radical profile peak locations (Benezech, Bergthorson & Dimotakis 2009), and show that the Δz_{CH} values have lower associated uncertainties than the corresponding ΔS_u values.

6. Conclusions

Studies of axisymmetric, jet-wall stagnation flames can provide accurate data for the validation of combustion chemical kinetic models. Such validations require a detailed understanding of the hydrodynamics of these flames, and this paper has demonstrated several key properties of these flows that are important for future flame studies.

Stagnation flame velocity profiles are found to be independent of the nozzle-to-plate separation distance when the Bernoulli velocity is held constant. This is consistent with results found for cold impinging jets and indicates that it is the imposed pressure drop across the nozzle that determines the stagnation flame flowfield and resulting strain rate. This indicates that care must be taken when defining a global strain rate, typically chosen to be the jet velocity divided by the nozzle-to-plate separation distance in such a geometry, if a contraction nozzle is used to generate the flow. Recent studies have shown that large uncertainties in the extinction strain rate result due to uncertainties in the upstream nozzle-exit boundary condition (Ji *et al.* 2010). The fact that the strain rate depends only on the Bernoulli velocity and is not influenced by the separation distance between the nozzle and stagnation surface or the exact value of the flame speed and flame position can be used to accurately specify the strain rate imposed on the experiment.

The hydrodynamic model of stagnation flames developed by Matalon and co-workers relies on large activation energy asymptotic methods and has been shown to yield reasonable agreement with reference flame speed values, but over-predicts the flame standoff distance due to the fact that the experiments have a thermal boundary layer where heat is lost to the wall. This model requires the velocity gradient in the unburned region to be specified from experiment, but all other model parameters are fundamental flame properties that can be calculated using equilibrium thermodynamics and laminar flame codes with appropriate choice of combustion chemistry, thermodynamic and transport models. This model has been extended in the present paper by introducing the error function model for the cold flow upstream of the flame, which is fully specified by the Bernoulli velocity. The extended model also accounts for the wall boundary-layer displacement thickness and the finite thickness of the velocity transition from the unburned to burned regions that results from the finite thickness of the temperature profile using the formulation of Tien & Matalon (1991). The predicted flame locations of the model are in good agreement with measurements for flames well-separated from the stagnation surface when the effect of the thermal boundary layer is accounted for.

Flames are studied with variable nitrogen dilution to change the flame strength without significantly altering the combustion chemistry. With increasing nitrogen dilution, the flame speed decreases and the flame moves towards the stagnation wall. For fixed U_B, the strain rate stays constant and the post-flame velocity profiles collapse, confirming that it is the nozzle pressure drop that determines the flame strain rate regardless of the flame stand-off distance or the exact value of the flame speed. Good agreement is observed between numerical simulation and experiment with

increasing nitrogen dilution, indicating that the flow and chemistry models are able to accurately account for the effect of variable dilution when inlet velocity boundary conditions are specified from the measured profiles. This can allow strong-burning flames to be diluted in order to facilitate their study.

The relative agreement between simulation and experiment is also not affected by the value of the strain rate used for the flames studied. Good agreement is found for slightly-lean methane flames using the GRI-Mech 3.0 combustion model and for lean ethylene flames using the SD2005 model. However, the DLW99 mechanism predicts lower flame speeds for lean ethylene flames than observed in experiments, which leads to deviations between the predictions of either the analytical model or detailed numerical simulations with experiment. The numerical simulations accurately predict the variation of the reference flame speed with strain rate, which is larger than that predicted by the analytical model. The fact that the deviations observed do not depend on the specific value of the strain rate imposed upon the flame, for all but the highest strain rates where the flame is close to extinction due to its proximity to the cold stagnation wall, is important because it means a single experiment at each equivalence ratio can be used to validate combustion models. This is consistent with recent work by Egolfopoulos and co-workers (Wang *et al.* 2009; Ji *et al.* 2010; Veloo *et al.* 2010), where a nonlinear extrapolation technique is used to determine the experimental laminar flame speed value. The nonlinear extrapolation method proposed by those authors is equivalent to assuming that differences between simulated and measured reference flame speeds are equal to differences between the simulated and true laminar flame speed of the mixture, i.e. $\Delta S_u = \Delta S_f^0$.

In the analytical model, the flame standoff distance is proportional to the hydrodynamic length, which is defined as the ratio of the flame speed to the strain rate in the flow, $K = (\mathrm{d}u/\mathrm{d}z)_u$. Differences in flame position and flame speed in the stagnation flame geometry are thus directly correlated due to the linear velocity profile upstream of the flame. The two metrics for simulation performance used in this study, Δz_{CH} and ΔS_u, yield equivalent results. Thus, for stagnation flames, the flame, or CH-radical peak, position can be used as a secondary measure that can provide improved fidelity in model validation studies.

The use of direct comparisons of model predictions to experiment provides an important means to validate models while minimizing the effect of the uncertainties that are inherent in any experiment. The ability to directly compare profile measurements in stagnation flame experiments with simulations allows the incorporation of additional diagnostic techniques to further probe model predictions. For example, flame speeds, intermediate species concentrations, major species concentrations and temperatures could be measured simultaneously, or sequentially, in a stable, steady flame that can be accurately modelled with detailed chemistry. Such measurements would provide a stringent validation criterion and allow the development of increasingly robust combustion models. The improved understanding of stagnation flame hydrodynamics discussed in this paper can be exploited to improve the experimental approaches used in future flame studies.

We acknowledge fruitful discussions with K. Sone and L. Benezech, as well as assistance by D. Lang with digital imaging and D. Goodwin with the CANTERA software package. Several stagnation flame computations were carried out using the 'Consortium Laval, Université du Québec, McGill and Eastern Quebec' (CLUMEQ) super-computing facilities. The work was funded by the Air Force Office of Scientific Research, the Natural Sciences and Engineering Research Council of Canada, the

Canada Foundation for Innovation and the 'Fonds Québécois de la Recherche sur la Nature et les Technologies', whose support is gratefully acknowledged.

Appendix. 1-D modelling and simulations of stagnation flames

Numerical simulations are performed using the CANTERA software package for reacting flow (Goodwin 2003; Bergthorson *et al.* 2005*a*). The 1-D solution approximates the stagnation flow in terms of a streamfunction, $\psi(z,r)=r^2U(z)$, with $U(z)=\rho u/2$, where u is the axial velocity (Kee *et al.* 1988). The axisymmetric momentum equation then becomes

$$2\,U\frac{\mathrm{d}}{\mathrm{d}z}\left(\frac{1}{\rho}\frac{\mathrm{d}U}{\mathrm{d}z}\right)-\frac{1}{\rho}\left(\frac{\mathrm{d}U}{\mathrm{d}z}\right)^2-\frac{\mathrm{d}}{\mathrm{d}z}\left[\mu\frac{\mathrm{d}}{\mathrm{d}z}\left(\frac{1}{\rho}\frac{\mathrm{d}U}{\mathrm{d}z}\right)\right]=\Lambda. \tag{A 1}$$

where μ is the viscosity of the gas and, in this formulation, $\Lambda=(1/r)\,\mathrm{d}p/\mathrm{d}r$ must be a constant. If the potential-flow boundary condition is used, then $\Lambda=-\rho\,(\mathrm{d}u/\mathrm{d}z)_u^2/4$ and the inviscid outer solution of (A 1) is an axial velocity profile with a constant gradient. By treating Λ as unspecified, the velocity and velocity gradient can be specified at the two boundaries of the simulation domain, $z=0$ and $z=\ell$, with $0<\ell\leqslant L$ a suitably chosen interior point in the flow. The velocity, u, and velocity gradient, $u'=(\mathrm{d}u/\mathrm{d}z)$, are set to zero at the stagnation wall, $z=0\,\mathrm{mm}$, in order to satisfy the no-penetration and no-slip conditions.

The streamfunction formulation used to derive the 1-D hydrodynamic model constrains the axial velocity to have no radial dependence, while the radial velocity must be a linear function of the radial coordinate (Seshadri & Williams 1978). Figure 18 shows the axial and radial velocity profiles as a function of the radial coordinate for several axial locations through the stagnation flame. Near the nozzle location, the axial velocity exhibits the 'top hat' velocity profile typical of high-contraction-ratio nozzles. The radial velocity is negligible at this location. As the flow approaches the flame, the stagnation flow induced by the virtual stagnation point arising from the flame dilatation causes the streamlines to diverge and induces a constant radial velocity gradient over the central region of the flame ($\approx$70 % of the nozzle diameter). The axial velocity profile begins to be decelerated at the central region of the jet compared to the outer edges of the flow, an effect seen even at $L/D=0.99$ for this flame location. Following the flame and its attendant heat release, the axial velocity profile becomes very flat over the radial domain. As the flow approaches the wall, a decrease in axial velocity is accompanied by an increase in the radial velocity gradient. These results are consistent with that observed in previous studies of non-reacting and reacting stagnation flows (Mendes-Lopes & Daneshyar 1985; Rolon *et al.* 1991). 2-D direct numerical simulations also show a linear radial velocity profile for over 60 % of the radial domain (Sone 2007). The linear radial velocity profiles found in experiment and 2-D simulations indicate that the assumptions that underpin the 1-D hydrodynamic model, used in both the analytical modelling and numerical simulation approaches discussed in this paper, are accurate for experimental stagnation flames.

In order to accurately compare such simulations with experiment, it is essential that the velocity boundary conditions at the simulation inlet, $z=\ell$, are specified in a consistent and robust manner, as simulated flame profiles with the same cold-flow strain rate exhibit different flame stand-off distances and profile shapes depending on the upstream boundary condition choice (Libby & Smooke 1997; Davis, Quinard & Searby 2001; Kee *et al.* 2003). Potential-flow boundary conditions will typically not

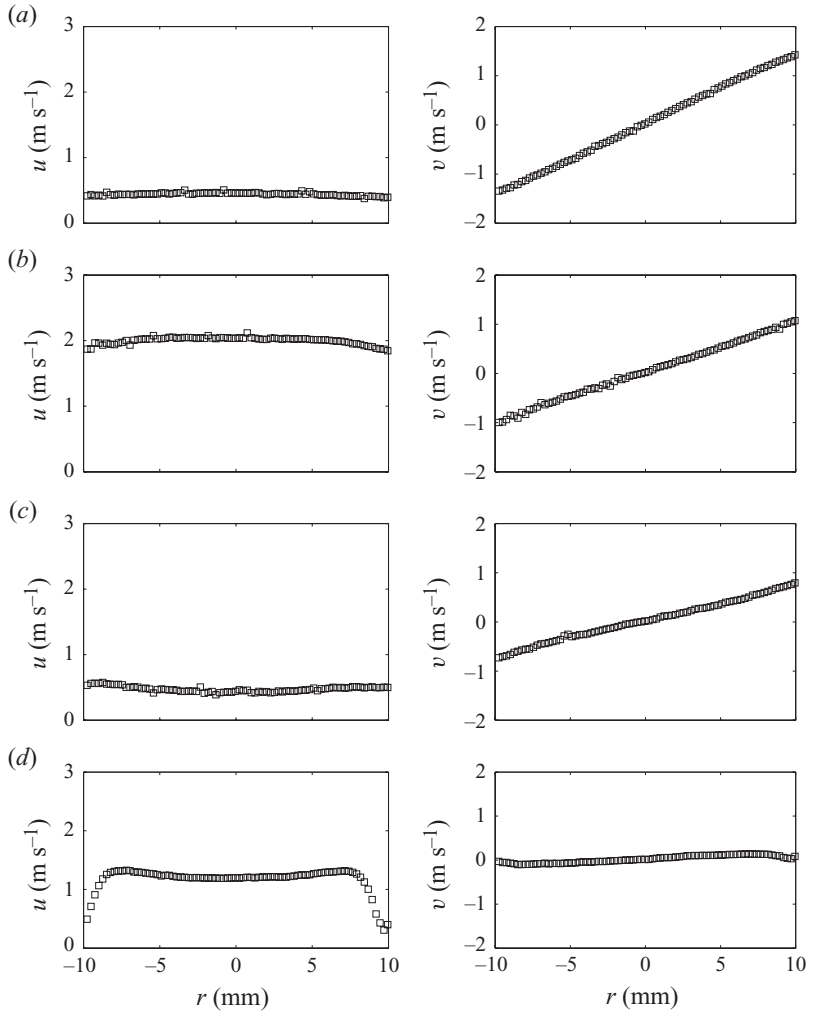

FIGURE 18. Axial (left) and radial (right) velocity measurements as a function of the radial coordinate for a stoichiometric methane–air flame with a nozzle exit velocity of $1.28\,\mathrm{m\,s^{-1}}$, diameter of $D = 20\,\mathrm{mm}$ and separation distance of $L = 20\,\mathrm{mm}$ ($L/D = 1$). Figures obtained at normalized axial locations, z/D, of: (*a*) 0.08, (*b*) 0.40 (*c*) 0.64 and (*d*) 0.99, corresponding to locations just upstream of the wall, sightly downstream of the flame, slightly upstream of the flame, and close to the nozzle exit, respectively.

match the experimental profile in the cold flow region, except for a short-distance upstream of the flame (see figures 2 and 5, and, for example, Eteng *et al.* 1986; Sung *et al.* 1996*a*). The radial velocity at the nozzle exit can be forced to be zero if a porous metal burner, or similar device, is used to deliver the flow. This results in the so-called 'plug flow' boundary condition, where $u'(L) = 0$ (Williams 2000). Frouzakis *et al.* (1998) performed 2-D direct numerical simulations of opposed-jet diffusion flames in an axisymmetric flow geometry. These authors utilized both parabolic and plug-flow boundary conditions at the jet exits and found that the 1-D streamfunction with plug-flow boundary conditions can adequately model the flow if the nozzle-exit profile is uniform, up to a nozzle-diameter to nozzle-separation-distance ratio of 1. However, high-contraction-ratio nozzles are used in the majority of studies that

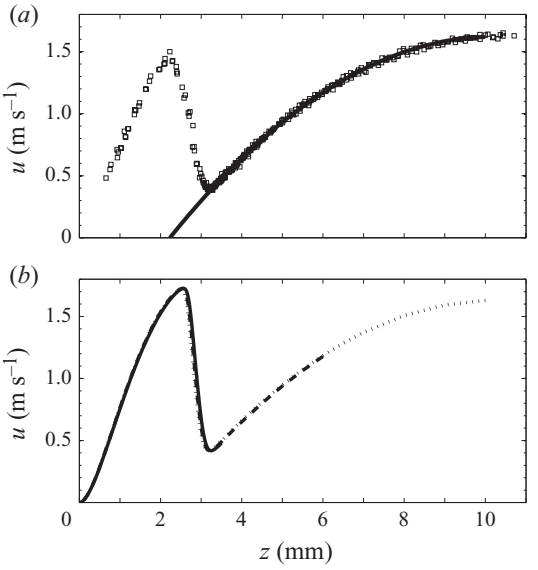

FIGURE 19. (*a*) Parabolic fit (solid line) to PSV data (□) for a $\Phi = 0.9$ methane–air flame at $L/d = 1.2$. (*b*) Simulated flame profiles using GRI-Mech 3.0 with $\ell =$ 3.5 mm (solid), 6 mm (dashed) and 10 mm (dotted).

employ particle seeding for velocimetry measurements in such flames and it has been shown that plug flow boundary conditions cannot capture the flow profiles for any ℓ or L values in contraction-nozzle-generated flows (Bergthorson *et al.* 2005*b*).

The axisymmetric 1-D stagnation flow hydrodynamic model has been validated against velocity profile measurements and axisymmetric 2-D direct numerical simulations of non-reacting impinging laminar jets (Bergthorson *et al.* 2005*b*). The stagnation flow model yields good agreement with both experiment and 2-D direct numerical simulations if inlet velocity and velocity gradient boundary conditions are specified at an interior location in the flow domain, $0 < \ell < 0.8D$ (Bergthorson *et al.* 2005*b*). If Λ is allowed to vary, the non-reacting, inviscid solution to the streamfunction model becomes a parabola (Seshadri & Williams 1978), and thus a parabola is fit to the velocity data in the cold region upstream of the flame (Bergthorson *et al.* 2005*a*; Bergthorson & Dimotakis 2007). Velocity data from a near-stoichiometric methane–air flame and the corresponding parabolic fit are given in figure 19(*a*). The velocity boundary conditions, $u(\ell)$ and $u'(\ell)$, are calculated from the parabolic fit at $z = \ell$, minimizing errors that could be introduced from data differentiation by utilizing all velocity measurements in the cold flow region. Simulated velocity profiles resulting from different choices of the simulation domain, ℓ, are presented in figure 19(*b*), using the GRI-Mech 3.0 chemical kinetic model. The predicted flame profiles are insensitive to the choice of ℓ, validating the use of the parabolic fit in specifying the inlet velocity boundary conditions.

Figure 20 compares the axial velocity and radial velocity gradient profiles for a stoichiometric methane–air flame to numerical simulation predictions using GRI-Mech 3.0. The radial velocity gradient profile is determined by performing linear regression on the radial PIV profiles, over a radial range where the profiles are linear, at each axial location (see figure 18). The axial velocity profile is predicted accurately for stoichiometric methane flames as observed previously (Bergthorson & Dimotakis 2007). The excellent agreement between the measured radial velocity

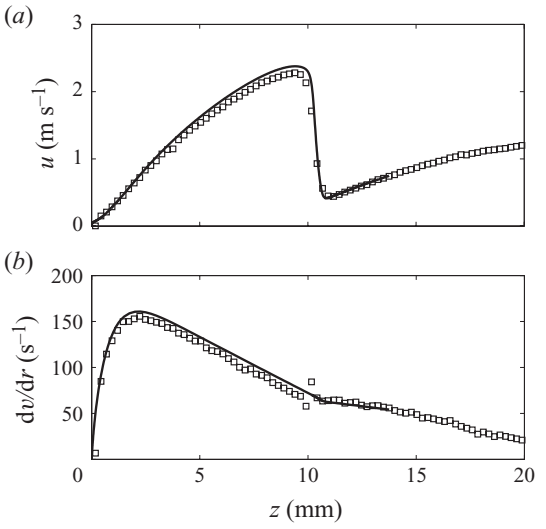

FIGURE 20. Stoichiometric methane–air flame profiles simulated with GRI-Mech 3.0. (*a*) Axial velocity profiles, and (*b*) radial velocity gradient profiles. PSV data (□) and simulations (solid lines).

gradient profile and the numerical simulation is further evidence of the ability of the 1-D hydrodynamic model to accurately model stagnation flame experiments. These results collectively indicate that the approximations used to derive the 1-D hydrodynamic model are valid over a significant portion of the flow domain and that this hydrodynamic model can be accurately used in analytical modelling and numerical simulation of stagnation flames if the inlet velocity boundary conditions are appropriately specified.

REFERENCES

BENEZECH, L. J., BERGTHORSON, J. M. & DIMOTAKIS, P. E. 2009 Premixed laminar C_3H_8- and C_3H_6–air stagnation flames: experiments and simulations with detailed kinetic models. *Proc. Combust. Inst.* **32**, 1301–1309.

BERGTHORSON, J. M. 2005 Experiments and modeling of impinging jets and premixed hydrocarbon stagnation flames. PhD thesis, California Institute of Technology, http://resolver.caltech.edu/CaltechETD:etd-05242005-165713.

BERGTHORSON, J. M. & DIMOTAKIS, P. E. 2006 Particle velocimetry in high-gradient/high-curvature flows. *Exp. Fluids* **41**, 255–263.

BERGTHORSON, J. M. & DIMOTAKIS, P. E. 2007 Premixed laminar C_1–C_2 stagnation flames: experiments and simulations with detailed thermochemistry models. *Proc. Combust. Inst.* **31**, 1139–1147.

BERGTHORSON, J. M., GOODWIN, D. G. & DIMOTAKIS, P. E. 2005*a* Particle streak velocimetry and CH laser-induced fluorescence diagnostics in strained, premixed, methane–air flames. *Proc. Combust. Inst.* **30**, 1637–1644.

BERGTHORSON, J. M., SONE, K., MATTNER, T. W., DIMOTAKIS, P. E., GOODWIN, D. G. & MEIRON, D. I. 2005*b* Impinging laminar jets at moderate Reynolds numbers and separation distances. *Phys. Rev.* E **72** (6), 066307, 1–12.

CHONG, C. T. & HOCHGREB, S. 2011 Measurements of laminar flame speeds of liquid fuels: Jet-A1, diesel, palm methyl esters and blends using particle imaging velocimetry (PIV). *Proc. Combust. Inst.* **33**, 979–986.

CONNELLY, B. C., BENNETT, B. A. V., SMOOKE, M. D. & LONG, M. B. 2009 A paradigm shift in the interaction of experiments and computations in combustion research. *Proc. Combust. Inst.* **32**, 879–886.

Davis, S. G., Law, C. K. & Wang, H. 1999 Propene pyrolysis and oxidation kinetics in a flow reactor and laminar flames. *Combust. Flame* **119**, 375–399.

Davis, S. G., Quinard, J. & Searby, G. 2001 A numerical investigation of stretch effects in counterflow, premixed laminar flames. *Combust. Theor. Model.* **5**, 353–362.

Durbin, P. A. 1982 The premixed flame in uniform straining flow. *J. Fluid Mech.* **121**, 141–161.

Egolfopoulos, F. N., Zhang, H. & Zhang, Z. 1997 Wall effects on the propagation and extinction of steady, strained, laminar premixed flames. *Combust. Flame* **109**, 237–252.

Eteng, E., Ludford, G. S. S. & Matalon, M. 1986 Displacement effect of a flame in stagnation-point flow. *Phys. Fluids* **29**, 2172–2180.

Frouzakis, C. E., Lee, J., Tomboulides, A. G. & Boulouchos, K. 1998 Two-dimensional direct numerical simulation of opposed-jet hydrogen–air diffusion flame. *Proc. Combust. Inst.* **27**, 571–577.

Goodwin, D. G. 2003 An open-source, extensible software suite for CVD process simulation. In *Proc. CVD XVI and EuroCVD 14*, Electrochemical Society, pp. 155–162.

Grcar, J. F., Kee, R. J., Smooke, M. D. & Miller, J. A. 1986 A hybrid Newton/time-integration procedure for the solution of steady, laminar, one-dimensional, premixed flames. *Proc. Combust. Inst.* **21**, 1773–1782.

Hirasawa, T., Sung, C. J., Joshi, A., Yang, Z., Wang, H. & Law, C. K. 2002 Determination of laminar flame speeds using digital particle image velocimetry: binary fuel blends of ethylene, *n*-butane, and toluene. *Proc. Combust. Inst.* **29**, 1427–1434.

Ishizuka, S. & Law, C. K. 1982 An experimental study on extinction and stability of stretched premixed flames. *Proc. Combust. Inst.* **19**, 327–335.

Ishizuka, S., Miyasaka, K. & Law, C. K. 1982 Effects of heat loss, preferential diffusion, and flame stretch on flame-front instability and extinction of propane/air mixtures. *Combust. Flame* **45**, 293–308.

Ji, C., Dames, E., Wang, Y. L., Wang, H. & Egolfopoulos, F. N. 2010 Propagation and extinction of premixed C_5–C_{12} *n*-alkane flames. *Combust. Flame* **157**, 277–287.

Kee, R. J., Coltrin, M. E. & Glarborg, P. 2003 *Chemically Reacting Flow – Theory and Practice.* John Wiley & Sons.

Kee, R. J., Miller, J. A., Evans, G. H. & Dixon-Lewis, G. 1988 A computational model of the structure and extinction of strained, opposed flow, premixed methane–air flames. *Proc. Combust. Inst.* **22**, 1479–1494.

Kim, Y. D. & Matalon, M. 1988 Propagation and extinction of a flame in a stagnation-point flow. *Combust. Flame* **73**, 303–313.

Law, C. K. 1988 Dynamics of stretched flames. *Proc. Combust. Inst.* **22**, 1381–1402.

Law, C. K. & Sung, C. J. 2000 Structure, aerodynamics, and geometry of premixed flamelets. *Prog. Energy Combust. Sci.* **26**, 459–505.

Law, C. K., Sung, C. J., Yu, G. & Axelbaum, R. L. 1994 On the structural sensitivity of purely strained planar premixed flames to strain rate variations. *Combust. Flame* **98**, 139–154.

Libby, P. A. & Smooke, M. D. 1997 The computation of flames in stagnation flows. *Combust. Sci. Technol.* **127**, 197–211.

Libby, P. A. & Williams, F. A. 1983 Strained premixed laminar flames under nonadiabatic conditions. *Combust. Sci. Technol.* **31**, 1–42.

Matalon, M., Cui, C. & Bechtold, J. K. 2003 Hydrodynamic theory of premixed flames: effects of stoichiometry, variable transport coefficients and arbitrary reaction orders. *J. Fluid Mech.* **487**, 179–210.

Matalon, M. & Matkowsky, B. J. 1982 Flames as gasdynamic discontinuities. *J. Fluid Mech.* **124**, 239–259.

Mendes-Lopes, J. M. C. & Daneshyar, H. 1985 Influence of strain fields on flame propagation. *Combust. Flame* **60**, 29–48.

Rolon, J. C., Veynante, D., Martin, J. P. & Durst, F. 1991 Counter jet stagnation flows. *Exp. Fluids* **11**, 313–324.

Salusbury, S. D. 2010 Premixed methane stagnation flames with oxygen enrichment. Master's thesis, McGill University, PID 87008, http://digitool.Library.McGill.CA:80/R/-?func=dbin-jump-full&object_id=87008&current_base=GEN01.

San Diego Mechanism 2005 http://maeweb.ucsd.edu/combustion/cermech/.

Schlichting, H. 1960 *Boundary Layer Theory.* McGraw-Hill, Inc.

Seshadri, K. & Williams, F. A. 1978 Laminar flow between parallel plates with injection of reactant at high Reynolds number. *Intl J. Heat and Mass Transfer* **21**, 251–253.

Sivashinsky, G. I. 1976 On a distorted flame front as a hydrodynamic discontinuity. *Acta Astronaut.* **3**, 889–918.

Smith, G. P., Golden, D. M., Frenklach, M., Moriarty, N. W., Eiteneer, B., Goldenberg, M., Bowman, C. T., Hanson, R. K., Song, S., Gardiner, W. C., Jr., Lissianski, V. V. & Qin, Z. 1999 GRI-Mech 3.0. http://www.me.berkeley.edu/gri_mech/.

Sone, K. 2007 Modeling and simulation of axisymmetric stagnation flames. PhD thesis, California Institute of Technology, http://resolver.caltech.edu/CaltechETD:etd-04252007-170838.

Sung, C. J., Kistler, J. S., Nishioka, M. & Law, C. K. 1996*a* Further studies on effects of thermophoresis on seeding particles in LDV measurements of strained flames. *Combust. Flame* **105**, 189–201.

Sung, C. J., Law, C. K. & Axelbaum, R. L. 1994 Thermophoretic effects on seeding particles in LDV measurements of flames. *Combust. Sci. Technol.* **99**, 119–132.

Sung, C. J., Liu, J. B. & Law, C. K. 1996*b* On the scalar structure of nonequidiffusive premixed flames in counterflow. *Combust. Flame* **106**, 168–183.

Tien, J. H. & Matalon, M. 1991 On the burning velocity of stretched flames. *Combust. Flame* **84**, 238–248.

Veloo, P. S., Wang, Y. L., Egolfopoulos, F. N. & Westbrook, C. K. 2010 A comparative experimental and computational study of methanol, ethanol, and *n*-butanol flames. *Combust. Flame* **157**, 1989–2004.

Wang, Y. L., Holley, A. T., Ji, C., Egolfopoulos, F. N., Tsotsis, T. T. & Curran, H. J. 2009 Propagation and extinction of premixed dimethyl-ether/air flames. *Proc. Combust. Inst.* **32**, 1035–1042.

Westbrook, C. K. & Dryer, F. L. 1981 Simplified reaction mechanisms for the oxidation of hydrocarbon fuels in flames. *Combust. Sci. Technol.* **27**, 31–43.

Williams, F. A. 2000 Progress in knowledge of flamelet structure and extinction. *Prog. Energy Combust. Sci.* **26**, 657–682.